Tendon and Motor Phenotypes in the *Crtap*$^{-/-}$ Mouse Model of Recessive Osteogenesis Imperfecta

Matthew W. Grol[1†], Nele A. Haelterman[1], Joohyun Lim[1], Elda M. Munivez[1], Marilyn Archer[2], David M. Hudson[2], Sara F. Tufa[3], Douglas R. Keene[3], Kevin Lei[1], Dongsu Park[1], David R. Eyre[2,] and Brendan H. Lee[1†]

[1] Department of Molecular and Human Genetics, Baylor College of Medicine, Houston, TX

[2] Department of Orthopaedics and Sports Medicine, University of Washington, Seattle, WA

[3] Shriners Hospital for Children, Portland, OR

[†] Correspondence and reprint requests:

Brendan H. Lee, Department of Human and Molecular Genetics, One Baylor Plaza, R814, Baylor College of Medicine, Houston, TX, USA, 77030, Email: blee@bcm.edu, Tel: +1 713-798-7246, Fax: +1 713-798-4523; Matthew W. Grol, Department of Physiology and Pharmacology, Dental Sciences Building, Room 0079, University of Western Ontario, London, ON, Canada, N6A 5C1, Email: mgrol2@uwo.ca, Tel: +1 519-661-2111 ext. 81060

Running Title: Tendon and motor deficits in Osteogenesis Imperfecta

Keywords: osteogenesis imperfecta, tendon, ligament, cross-link, motor behavior

ABSTRACT

Osteogenesis imperfecta (OI) is characterized by short stature, skeletal deformities, low bone mass with bone fragility, and motor deficits. A subset of OI patients also present with joint hypermobility; however, the role of tendon/ligament dysfunction in OI pathogenesis is largely unknown. Using the *Crtap*$^{-/-}$ mouse model of severe, recessive OI, we found that mutant Achilles tendons and patellar ligaments were thinner with increased collagen cross-links and reduced collagen fibril size at 1- and 4-months compared to wildtype. Patellar ligaments from *Crtap*$^{-/-}$ mice also had fewer progenitors with a concomitant increase in immature cells. RNA-seq analysis of Achilles tendons and patellar ligaments from 1-month *Crtap*$^{-/-}$ mice revealed dysregulation in matrix gene expression concomitant with predicted alterations in TGF-β, inflammatory, and metabolic signaling. Finally, a series of behavioral tests revealed severe motor impairments and reduced grip strength in 4-month *Crtap*$^{-/-}$ mice – a phenotype that correlates with the tendon/ligament pathology.

INTRODUCTION

Tendon is a fibrous tissue that connects skeletal muscle to bone to facilitate motion, whereas ligaments connect articulating bones to support joint alignment and function[1, 2]. The extracellular matrix of tendons/ligaments is primarily composed of type I collagen as well as smaller quantities of other collagens and proteoglycans[3]. During development, the collagen fibrils in tendons and ligaments develop through addition and lengthening before transitioning to the appositional fusion of existing fibers with continued lengthening in postnatal life[4]. The synthesis and assembly of this collagen-rich matrix are influenced by other small collagens and proteoglycans as well as by the cross-linking chemistry of type I procollagen fibrils, which in turn regulates fibril size and strength[5]. Like tendon and ligament, the organic matrix of bone consists largely of type I collagen[6], and disruptions in collagen synthesis and folding are known to negatively impact its biochemical and mechanical properties in connective tissue diseases such as Osteogenesis Imperfecta (OI)[7]. However, despite evidence of joint mobility phenotypes and motor deficits in OI patients[8, 9], tendon and ligament phenotypes in this disease are relatively understudied.

OI is a heterogeneous group of disorders characterized by variable short stature, skeletal deformities, low bone mass, and increased bone fragility. Approximately 80% of OI cases are caused by dominantly inherited mutations in the genes encoding the α1(I) or α2(I) chains of type I collagen. Mutations in genes responsible for the synthesis, post-translational modification, and processing of collagen, such as cartilage-associated protein (CRTAP), lead to severe, recessive forms of this disease[7]. In addition to skeletal defects, other connective tissue manifestations including joint hypermobility and skin hyperlaxity are observed in a subset of OI patients[8, 9]. Our and others' studies have shown that CRTAP forms a complex with Prolyl 3-hydroxylase 1

70 (P3h1, encoded by *Lepre1*) and Cyclophilin B (CypB, encoded by *Ppib*), and is required for
71 prolyl 3-hydroxylation of type I procollagen at Pro986 of chain α1(I) and Pro707 of chain
72 α2(I)[10-12]. In this regard, loss of either CRTAP or P3H1 leads to loss of this complex and its
73 activity, causing a severe recessive form of OI characterized by short stature and brittle bones[11,
74 13-15]. Collagen isolated from *Crtap*$^{-/-}$ and *Lepre1*$^{-/-}$ mice is characterized by lysine over-
75 modifications and abnormal fibril diameter[11, 14]. While a comprehensive analysis of *Crtap*$^{-/-}$ mice
76 has revealed multiple connective tissue abnormalities, including in lungs, kidneys, and skin[16], the
77 impact of the loss of Crtap on tendons and ligaments remains unknown.

78 Alterations in collagen fibril size and cross-linking have been noted in a limited number
79 of studies using dominant or recessive mouse models of OI[17-19]; however, whether loss of Crtap
80 impacts tendon and ligament development and structure remains unknown. In this study, we
81 show that *Crtap*$^{-/-}$ mice have thinner Achilles tendons and patellar ligaments at 1 and 4 months-
82 of-age that are hypercellular with a reduction in tendon progenitors and total ligament volume.
83 Moreover, the patellar and cruciate ligaments from *Crtap*$^{-/-}$ show increased cell size and variable
84 ectopic chondrogenesis by 4 months-of-age. Examining the collagen matrix, we found an
85 increase in stable (irreversible) collagen cross-links at both timepoints, accompanied by
86 alterations in fibril diameter at 4-months compared to wildtype controls. RNA-seq analyses
87 revealed both common and distinct changes in the transcriptome of the Achilles tendon and
88 patellar ligaments of *Crtap*$^{-/-}$ mice compared to wildtype with a predicted activation of
89 transforming growth factor-β (TGF-β) and inflammatory signaling in both tissues. These
90 changes in *Crtap*$^{-/-}$ tendons and ligaments were accompanied by motor deficits and reduced
91 strength at 4 months-of-age. In conclusion, loss of CRTAP in mice causes tendon/ligament
92 abnormalities and significant behavioral impairments.

93 **MATERIALS AND METHODS**

94 *Animals*

95 *Crtap*$^{-/-}$ mice were generated as previously described[11] and maintained on a mixed C57BL/6J
96 and 129Sv genetic background. All studies were performed with approval from the Institutional
97 Animal Care and Use Committee (IACUC) at Baylor College of Medicine. Mice were housed 3
98 to 4 mice to a cage in a pathogen-free environment with *ad libitum* access to food and water and
99 under a 14h light/10h dark cycle.

100

101 *Histological analysis*

102 Mice were euthanized and ankle and knee joints were dissected and fixed for 48 h on a shaker at
103 4ºC or room temperature in freshly prepared 4% paraformaldehyde (PFA) in 1×phosphate-
104 buffered saline (PBS). Samples were decalcified at 4°C using 10% ethylenediaminetetraacetic
105 acid (EDTA) in 1×PBS for 10 days (with one change out at 5 days) before paraffin embedding
106 using a standard protocol. Samples were sectioned at 6-µm and stained with hematoxylin and
107 eosin (H&E) to visualize tendon structures. Cell number per tissue area was determined using the
108 Fiji release of ImageJ[20].

109

110 *Fluorescence-activated cell sorting analysis of tendon progenitors*

111 After dissection of patellar ligaments from 5-month-old wildtype and *Crtap*$^{-/-}$ mice, tissues were
112 cut into small pieces in 1×PBS with 10% fetal bovine serum (FBS) and incubated with 500 µl of
113 PBS + 10% FBS and 0.1% collagenase at 37°C for 3 hours. After digestion, cells were filtered
114 with a 40-µm strainer, washed, resuspended in 1×PBS at a concentration of 10^6 cells/mL, and
115 stained with CD45-pacific blue (clone: 30-F11), CD31-eFlour 450 (clone: 390), CD146-PE-Cy7

116 (clone ME-9F1) and CD200-APC (clone OX-90) (eBioscience). Propidium iodide was used for
117 selecting viable cells. Cell analysis was performed using a LSRII Fortessa, and FACS
118 experiments were done using an AriaII cytometer (BD Biosciences, San Jose, CA). Data were
119 analyzed with FlowJo software (TreeStar, OR).
120
121 *Phase-contrast μCT imaging and analysis*
122 To quantify tendon/ligament volume, knee joints were dissected from mice, stained with contrast
123 agents, scanned by phase-contrast μCT, and analyzed using TriBON software (RATOC, Tokyo,
124 Japan) as previously described for articular cartilage[21-24]. In addition to the articular surfaces
125 (data not shown), we performed contrast-enhanced visualization of the patellar ligament using
126 this protocol. To quantify volume, samples were examined in transverse where the patellar
127 ligament boundary was easily distinguished from the joint capsule. Ligament volume was
128 assessed from its origin within the patella to its insertion at the tibia.
129
130 *Transmission electron microscopy analysis of collagen fibril size*
131 Mouse ankle and knee joints were dissected and fixed in fresh 1.5% glutaraldehyde/1.5% PFA
132 (Tousimis) with 0.05% tannic acid (Sigma) in 1×PBS at 4°C overnight to preserve the native
133 tension on relevant tendons/ligaments. The next day, flexor digitorum longus (FDL) and Achilles
134 tendons as well as patellar ligament were dissected out in 1×PBS, and placed back into fixative.
135 Samples were then post-fixed in 1% osmium tetroxide (OsO_4), rinsed in Dulbecco's Modified
136 Eagle Medium (DMEM), and dehydrated in a graded series of ethanol to 100%. Samples were
137 rinsed in propylene oxide, infiltrated in Spurrs epoxy, and polymerized at 70°C overnight. TEM
138 images were acquired using an FEI G20 TEM at multiple magnifications to visualize transverse

139 sections of collagen fibrils. Collagen fibril diameter was measured using the Fiji release of
140 ImageJ[20].
141
142 *Tendon collagen cross-linking analysis*
143 Collagen hydroxylysyl-pyridinoline (HP) cross-links were quantified as previously described[25,
144 26]. In brief, tendons and ligaments isolated from hindlimbs were hydrolyzed by 6M HCl for 24h
145 at 108°C. Dried samples were then dissolved in 1% (v/v) n-heptafluorobutyric acid for
146 quantitation of HP by reverse-phase HPLC with fluorescence monitoring.
147
148 *RNA-seq analysis*
149 At 1 month-of-age, Achilles tendons were excised using scissors proximal to the calcaneal
150 insertion and distal to the tendon-muscular-junction, whereas patellar ligaments were removed
151 via scalpel just proximal to the tibial insertion and distal to the patella. Tendons and ligaments
152 were not cleaned of their paratenon layers in either case. RNA extraction for both tissues was
153 performed with the Fibrous Connective Tissue kit (Qiagen), with columns from the RNeasy
154 Micro Kit (Qiagen) employed for the patellar ligament. Quality control, library preparation,
155 sequencing, and differential gene expression analysis including gene ontology analysis was
156 performed by GENEWIZ® (South Plainfield, NJ). For the examination of predicted Upstream
157 Regulators, we utilized the Ingenuity Pathway Analysis (IPA) platform (Qiagen) with an
158 adjusted *p*-value of 0.05. The expression is shown as Base Means and read counts of genes were
159 normalized per million transcripts (Transcripts Per Million; TPM).
160
161 *Open field assessment of spontaneous motor activity*

Open field activity was measured using the VersaMax Animal Activity Monitoring System (AccuScan Instruments, Columbus, OH). On the day of assessment, mice were transferred to the test room and allowed to acclimate in their home cage for 30 min at 50 Lux of illumination with 60 dB of white noise. Mice were then placed individually into clear 40 cm × 40 cm × 30 cm chambers and allowed to move freely for 30 min. Locomotion parameters and zones were recorded using the VersaMax activity monitoring software. Chambers were cleaned with 30-50% ethanol to remove the scent of previously tested mice between each run.

Rotarod analysis of motor coordination and endurance

On the day of assessment, mice were transferred to the test room and allowed to acclimate within their home cage for 30 min at 50 Lux of illumination with 60 dB of white noise. Mice were then placed on a rotarod (UGO Basile, Varese, Italy) set to accelerate from 5-to-40 RPM over 5 min. Five trials were performed per day for 2 consecutive days (trials 1-10) with a rest time of 5 min between trials. Latency to fall was recorded when the mouse fell from the rotating rod or went for two revolutions without regaining control. The rotarod was cleaned with 30-50% ethanol between mice to remove the scent of previously tested animals.

Grid foot slip analysis of motor coordination

The grid foot slip assay consisted of a wire grid set atop a stand where the movement was recorded by a suspended digital camera. Mice were transferred to the test room on the day of assessment and allowed to acclimate within their home cage for 30 min at 50 Lux of illumination with 60 dB of white noise. Mice were then placed one at a time on the grid and allowed to move freely for 5 min. The observer sat 6-8 feet away at eye-level to the mouse and recorded forelimb

185 and hindlimb foot slips using the ANY-maze video tracking software (Stoelting Co., Wood Dale,
186 IL). After the test, mice were removed to their original home cage. Forelimb and hindlimb foot
187 slips were normalized to the total distance traveled during the test.
188
189 *Inverted grid analysis of strength and endurance*
190 On the day of assessment, mice were transferred to the test room and allowed to acclimate within
191 their home cage for 30 min at 50 Lux of illumination with 60 dB of white noise. Mice were then
192 placed in the middle of a wire grid, held approximately 18-in above a cushioned pad, and
193 inverted. The latency to fall for each mouse was recorded. At the completion, mice were returned
194 to their home cage.
195
196 *Grip strength analysis*
197 Mice were transferred to the test room on the day of assessment and allowed to acclimate within
198 their home cage for 30 min at 50 Lux of illumination with 60 dB of white noise. Each mouse was
199 then lifted by its tail onto the bar of a digital grip strength meter (Columbus Instruments,
200 Columbus, OH). Once both forepaws had gripped the bar, the mouse was gently pulled away
201 from the meter by its tail at a constant speed until the forepaws were released. The grip (in N of
202 force) was recorded and the procedure repeated twice for a total of three measurements, which
203 were averaged for the final result.
204
205 *Statistical analysis*
206 Determination of sample size was based on previous publications. Biological replicates were
207 defined as an individual mouse for each experiment. Respective tendons and ligaments from the

208 left and right hindlimbs were combined for TEM, collagen cross-linking, tendon progenitor, and
209 RNA-seq analyses. Data are presented as means ± S.D. or min-to-max box and whisker plots
210 with individual data points. For data whose residuals passed the Shapiro-Wilk test for normality,
211 groups of two were compared using unpaired t-tests, and groups of three or more were compared
212 using one-way ANOVA followed by Tukey's post-hoc tests. For data whose residuals did not
213 have a normal distribution, groups of two were compared using a Mann-Whitney test, and groups
214 of three or more were compared using Kruskal-Wallis followed by Dunn's post-hoc tests. For the
215 Rotarod assay, where time was a variable, groups were compared using repeated measures two-
216 way ANOVA followed by Tukey's post-hoc tests. For all tests reported above, statistical analysis
217 was performed using Prism 8.3.1 (GraphPad Software, La Jolla, CA). For all tests, the exact *p*-
218 value is reported, and a *p*-value of < 0.05 was considered statistically significant.
219

220 **RESULTS**

221 *Crtap$^{-/-}$ mice exhibit abnormal tendon development*

222 Mice lacking Crtap present with growth delay, rhizomelia, and severe osteoporosis together with
223 disruption of other connective tissues including lung and skin[11, 16]. To assess whether *Crtap$^{-/-}$*
224 mice exhibit disruptions in the development of tendons and ligaments, we harvested ankle and
225 knee joints at 1 and 4 months-of-age to histologically examine the Achilles tendon and patellar
226 ligament. At 1-month, *Crtap$^{-/-}$* mice presented with thinner Achilles tendons and patellar
227 ligaments (**Figure 1C,F**) compared to wildtype (**Figure 1A,D**) and heterozygous mice (**Figure**
228 **1B,E**) with increased cell density in both structures (**Figure 1M**). There was also prominent
229 hyperplasia of the synovial membrane in *Crtap* mutant knees at this age (**Figure 1F**). By 4
230 months-of-age, *Crtap$^{-/-}$* Achilles tendons and patellar ligaments remained thinner and

231 hypercellular compared to wildtype and heterozygous mice (**Figure 1G-L,N**). In addition,
232 synovial hyperplasia persisted within *Crtap*$^{-/-}$ knees (**Figure 1L**). Interestingly, ectopic
233 chondrogenesis was present towards either end of the patellar ligament and/or cruciate ligaments
234 in some (but not all) 4-month-old *Crtap*$^{-/-}$ mice (**Figure 1L**) – a phenomenon that can occur in
235 tendinopathy[27].

236 To more accurately quantify the differences in tendon/ligament size between genotypes,
237 we performed phase-contrast μCT to examine differences in patellar ligament volume between
238 genotypes (**Figure 1O-Q**) – a technique we previously used to examine soft tissues including
239 articular cartilage in intact murine knee joints[21-24]. In 4-month-old mice, we observed a thinning
240 of the patellar ligament compared to wildtype mice, with no notable changes in articular cartilage
241 surface (**Figure 1O,P**). Confirming our histological findings, quantification revealed a decrease
242 in patellar ligament volume in *Crtap*$^{-/-}$, but not in heterozygous mice, compared to wildtype
243 controls (**Figure 1Q**).

244 Postnatal progenitor populations are thought to be critical for the maintenance and
245 regeneration of tendon/ligament tissue. Previous studies have shown that a subset of fibroblasts
246 in the tendon midsubstance (endotenon) has the potential to contribute to tendon homeostasis and
247 regeneration at various developmental stages[28-30]. In addition, platelet-derived growth factor
248 receptor α (PDGFRa)$^{+}$ cells in the tendon sheath (paratenon) can contribute to tendon
249 regeneration after acute injury[31]. These progenitor cells can be labeled by *Tppp3*-CreER[31] or
250 *aSMA*-CreER[28] with the expression of tendon progenitor markers such as CD146[32], CD140a
251 (PDGFRa)[31], and CD200[33]. Given the significant hypercellularity seen in the Achilles tendons
252 and patellar ligaments from *Crtap*$^{-/-}$ mice, we examined whether the postnatal progenitor
253 population is altered compared to wildtype controls. Using fluorescence-activated cell sorting

254 (FACS) analysis of 5-month-old patellar ligaments, we observed a significant decrease in the
255 percentage of $CD45^{-}CD31^{-}CD146^{+}CD200^{+}$ stem/progenitor cells (~2%) compared to wild-type
256 mice (~4%) (**Figure 2A-C**, red box), while $CD45^{-}CD31^{-}CD146^{-}CD200^{+}$ immature cells were
257 concomitantly increased in *Crtap*$^{-/-}$ mice (**Figure 2D**).

258 Taken together, these data demonstrate that *Crtap*$^{-/-}$ mice display disruptions in the
259 development and postnatal maturation of tendons and ligaments. Moreover, the matrix
260 disruptions caused by loss of CRTAP lead to the dysregulation of the postnatal tendon progenitor
261 pool as well as tenocyte maturation.

262

263 *Collagen fibril formation is altered in heterozygous and Crtap*$^{-/-}$ *mice*

264 Tendons develop embryonically by increasing fibril length and number, whereas postnatal
265 growth arises from an increase in fibril length and diameter – the latter of which is driven by the
266 lateral fusion of smaller fibrils[4]. To investigate the role of Crtap in collagen fibril maturation, we
267 utilized transmission electron microscopy (TEM) to examine changes in fibril diameter in flexor
268 digitorum longus (FDL) and Achilles tendons as well as patellar ligaments (**Figure 3**). In the
269 FDL tendon, there was a marked increase in small collagen fibrils (20-60 nm in size), a reduction
270 in 80-320 nm fibrils, and a slight increase in larger fibrils (>340 nm in diameter) in *Crtap*$^{-/-}$ mice
271 compared to wildtype (**Figure 3A,C,D**). Despite similarities seen in histology, heterozygous
272 mutant FDL tendons also exhibited a slight increase in 20-40 nm fibrils in mice compared to
273 wildtype controls (**Figure 3A-B,D**). Similar trends were observed for the Achilles tendon,
274 namely an increase in small fibrils (20-60 nm), a reduction in 80-240 nm fibrils, and an increase
275 in large fibrils (>280 nm) upon loss of *Crtap* (**Figure 3E,G-H**). In contrast to what we observed
276 for the FDL, heterozygous Achilles tendons did not have increased numbers of smaller fibers

277 (**Figure 3F,H**). Instead, a greater number of fibrils ranging from 140-200 nm in size were noted
278 compared to wildtype controls.

279 Compared to the FDL and Achilles tendons, the greatest differences were seen within the
280 patellar ligament, though the pattern of changes remained consistent (**Figure 3I-L**). Specifically,
281 we observed a dramatic increase in 20 nm collagen fibrils compared to both heterozygous and
282 wildtype mice (**Figure 3I-L**). Fibrils ranging from 100-180 nm in diameter were reduced in
283 heterozygous and *Crtap*$^{-/-}$ mice compared to wildtype. Interestingly, the greatest difference from
284 wildtype was an increase in large collagen fibrils (>200 nm) in both heterozygous and *Crtap*$^{-/-}$
285 mice (**Figure 3I-L**). Taken together, these data indicate that heterozygous and complete loss of
286 CRTAP alter collagen fibril assembly in tendons and ligaments. In addition, the degree to which
287 collagen assembly is affected is site-dependent.

288

289 *Collagen cross-linking is increased in heterozygous and Crtap*$^{-/-}$ *mice*

290 Along with P3H1 and CyPB, CRTAP is an integral part of the collagen prolyl 3-hydroxylation
291 complex that is responsible for the 3-hydroxylation of Pro986 of the type I procollagen α1
292 chain[7]. Loss of this complex blocks 3-hydroxyproline formation and affects lysine hydroxylation
293 and cross-linking in bone collagen[11, 12]; however, whether *Crtap*$^{-/-}$ tendons and ligaments display
294 altered collagen cross-linking is unknown. To investigate this, we harvested tendons and
295 ligaments at 1- and 4-months and assessed collagen cross-linking by quantifying the levels of
296 hydroxylysyl-pyridinoline (HP) (**Figure 4**). Overall, we observed an increase in these stable,
297 mature collagen cross-links from 1 to 4 months-of-age in all genotypes for the FDL and Achilles
298 tendons (**Figure 4A-B**). In contrast, for the patellar ligament, age-dependent increases in
299 collagen cross-links were only observed in *Crtap*$^{-/-}$ mice (**Figure 4C**). For FDL tendons, *Crtap*$^{-/-}$

300 mice had more of these collagen cross-links at 1- and 4-months compared to heterozygous and
301 wildtype mice; however, the content of HP residues per collagen decreased with age in this tissue
302 (**Figure 4A**). Interestingly, in Achilles tendons, an increase in collagen cross-linking was
303 observed in both heterozygous and *Crtap*$^{-/-}$ mice at 1-month compared to wildtype. In contrast, at
304 4-months, only *Crtap*$^{-/-}$ mice had elevated collagen cross-links, and these levels were greater than
305 those observed at the earlier time point (**Figure 4B**).
306 Of the tissues examined, the patellar ligament showed the greatest increase in collagen
307 cross-links both with time and across genotypes. Specifically, collagen cross-links were elevated
308 by 5- to 10-fold in *Crtap*$^{-/-}$ patellar ligaments compared to heterozygous and wildtype at 1- and
309 4-months, respectively (**Figure 4C**). Taken together, these data suggest that *Crtap* is required for
310 proper hydroxylation and cross-linking of collagen fibrils in tendons and ligaments in a semi-
311 dominant fashion, as heterozygous mutant tendons/ligaments display a phenotype that is milder
312 than the phenotype observed for homozygous mutant mice. Importantly, the chemical quality of
313 collagen cross-linking appears to be spatiotemporally regulated and this regulation is
314 differentially affected by the loss of a single or both copies of *Crtap*.
315
316 *Signaling and metabolic dysregulation in Crtap*$^{-/-}$ *tendons and ligaments*
317 To investigate the molecular changes underlying tendon/ligament phenotypes, we performed
318 bulk RNA-seq with RNA isolated from Achilles tendons and patellar ligaments of 1-month-old
319 wildtype and *Crtap*$^{-/-}$ mice. To determine global changes in differentially expressed genes as well
320 as predicted upstream regulators, we performed Ingenuity Pathway Analysis (IPA, Qiagen,
321 Germany). For the Achilles tendon, a total of 178 genes (consisting of 99 upregulated genes and
322 79 downregulated genes) were significantly differentially expressed between wildtype and *Crtap*$^{-}$

323 $^{-/-}$ samples (**Figure 5A**). Of the top 30 differentially expressed genes, several extracellular matrix
324 proteins, including matrilin-3 (*Matn3*), matrilin-4 (*Matn4*), and fibronectin 1 (*Fn1*), and
325 proteolytic enzymes such as matrix metallopeptidase 2 (*Mmp2*) were dysregulated. Gene
326 ontology analysis revealed "GO:000715 – Cell Adhesion", "GO:0045778 – Positive Regulation
327 of Ossification", and "GO:0051928 – Positive Regulation of Calcium Ion Transport" to be
328 enriched (**Figure 5B**). Examination of upstream regulators based on the differential gene
329 expression data also revealed a predicted activation of TGF-β1 in *Crtap*$^{-/-}$ mice and predicted
330 inhibition of dystrophin (DMD) along with several for which activation state was unclear,
331 including platelet-derived growth factor-BB (PDGF-BB), β-catenin (CTNNB1), and tumor
332 necrosis factor (TNF) (**Figure 5C**).
333 In keeping with the increased severity seen in ligaments from *Crtap*$^{-/-}$ mice compared to
334 tendons, a greater number of total genes were differentially expressed between wildtype and
335 *Crtap*$^{-/-}$ patellar ligament samples (**Figure 5D**). Specifically, we saw significant differential
336 expression of 519 genes, with 224 being upregulated and 295 downregulated in *Crtap*$^{-/-}$
337 compared to wildtype. Several of the top 30 differentially expressed genes were small collagens
338 such as type IX collagen α3 chain (*Col9a3*), type IX collagen α1 chain (*Col9a1*), and type XXII
339 collagen α1 chain (*Col22a1*) as well as other extracellular matrix proteins, including lumican
340 (Lum) and fibronectin 1 (*Fn1*). Unlike the Achilles tendon, gene ontology analysis revealed
341 significant enrichment for metabolic processes, including "GO:0055114 – Oxidation-Reduction
342 Process", "GO:0050873 – Brown Fat Cell Differentiation", and "GO:0050872 – White Fat Cell
343 Differentiation" as well as for "GO:0008284 – Positive Regulation of Proliferation" and
344 "GO:0001525 – Angiogenesis" (**Figure 5E**). Examination of upstream regulators also suggested
345 a highly significant activation of TNF and interleukin 6 (IL-6) as well as fibroblast growth factor

346 2 (FGF2) and TGF-β3 in *Crtap*$^{-/-}$ patellar ligaments (**Figure 5F**). Indeed, the representation of
347 TNF, TGF-β, and PDGF-BB in the ligament dataset is consistent with but more severe than that
348 observed for those same regulators in the Achilles tendon results (**Figure 5C**).
349
350 *Loss of CRTAP leads to deficiencies in motor activity, coordination, and strength*
351 To investigate whether the tendon phenotypes observed in *Crtap*$^{-/-}$ mice have functional
352 consequences, we performed a series of behavioral assays at 4 months-of-age. Using the open
353 field assay to quantify changes in spontaneous motor activity, we observed that *Crtap*$^{-/-}$ mice
354 displayed significant reductions in both horizontal and vertical activity compared to
355 heterozygous and wildtype mice (**Figure 6A-B**). We next examined changes in motor
356 coordination and endurance using the rotarod assay. While no genotype-dependent differences
357 were observed during the learning phase of the assessment (Trials 1-5), *Crtap*$^{-/-}$ displayed a
358 reduction in latency to fall for Trials 6, 9-10 compared to wildtype and Trials 6, 8-10 compared
359 to heterozygous mice (**Figure 6C**). To confirm this observation, we evaluated the mice using the
360 grid foot slip assay – an alternative metric for motor coordination. In this regard, we found that
361 *Crtap*$^{-/-}$ mice exhibited a modest increase in forelimb and hindlimb foot slips compared to
362 heterozygous and wildtype mice (**Figure 6D-E**). Taken together, these findings indicate that
363 *Crtap*$^{-/-}$ mice have deficiencies in motor activity and coordination compared to controls.
364 We next evaluated strength in the *Crtap*$^{-/-}$ mice using the inverted grid and grip strength
365 assays. Interestingly, we observed a decrease in the latency to fall during the inverted grid assay
366 for *Crtap*$^{-/-}$ mice compared to heterozygous and wildtype controls (**Figure 6F**). Using a more
367 quantitative metric, we examined these mice using the grip strength test and found that while
368 wildtype and heterozygous mice could generate approximately 1.3 N of force, mice lacking

369 CRTAP were weaker with a mean grip strength of 0.62 N (**Figure 6G**). Thus, *Crtap*$^{-/-}$ mice
370 display significant reductions in strength together with perturbations in motor activity and
371 coordination – behavioral changes that could be related in part to their tendon phenotype.
372

373 **DISCUSSION**

374 In this study, we examined the histological, ultrastructural, biochemical, and transcriptional
375 characteristics of tendons and ligaments in the *Crtap*$^{-/-}$ mouse model of severe, recessive OI. We
376 demonstrate that at 1- and 4 months-of-age, *Crtap*$^{-/-}$ have thinner, more cellular Achilles tendons
377 and patellar ligaments with a reduction in tendon progenitors compared to heterozygous and
378 wildtype mice. Using phase-contrast μCT imaging, we confirmed that tissue volume is reduced
379 in *Crtap*$^{-/-}$ patellar ligaments at 4-months than those from heterozygous and wildtype mice.
380 Examining collagen fibril organization, we found a marked alteration in small and large fibrils in
381 both heterozygous and *Crtap*$^{-/-}$ mice compared to wildtype that varied in severity depending on
382 the tendon or ligament being examined. Stable, HP cross-links were also elevated at 1- and 4-
383 months in *Crtap*$^{-/-}$ mice compared to wildtype, which indicates an increase in telopeptide lysine
384 hydroxylation and irreversible intermolecular cross-links (see below). RNA-seq analysis
385 revealed alterations in extracellular matrix proteins, growth factor signaling, and metabolic
386 pathways in *Crtap*$^{-/-}$ tendons and ligaments compared to wildtype controls. Finally, we
387 demonstrate that *Crtap*$^{-/-}$ mice exhibit motor impairments concomitant with reductions in grip
388 strength – a phenomenon that may be related to the tendon pathology observed in these mice.
389 Collagen ultrastructure and cross-linking has been well-documented in the bones of
390 mouse models for both dominant and recessive OI; however, quantitative differences in the
391 volume of tendons and ligaments in these models has not been examined and tendon/ligament

392 histological characterization has been modest. In this regard, we demonstrate that *Crtap*$^{-/-}$ mice
393 have thinner Achilles tendons and patellar ligaments at 1- and 4-months. Despite the reduction in
394 size and extracellular matrix, tendons and ligaments from these mice are hypercellular compared
395 to wildtype and heterozygous animals. At the same time, there is a significant reduction in
396 postnatal CD146+CD200+ tendon progenitors with a concomitant increase of immature cells.
397 While the alterations in tendon and ligament size and cellularity may be a result of alterations in
398 the collagen extracellular matrix, it could also be associated with alterations in cellular signaling.
399 In this regard, TGF-β signaling is upregulated in bones from *Crtap*$^{-/-}$ mice[34], and elevated TGF-β
400 signaling has been noted in mouse models with increased tendon cellularity and alterations in
401 collagen fibril distribution[35]. Indeed, our RNA-seq analysis identified TGF-β signaling as an
402 activated upstream regulator predicted to be driving differential gene expression observed in the
403 tendons and ligaments from *Crtap*$^{-/-}$ mice. We also observed significant metabolic dysregulation
404 in *Crtap*$^{-/-}$ ligaments. Interestingly, this a phenotype that has been observed in mammalian target
405 of rapamycin complex 1 (mTORC1) knockout mouse tendons that have a similar histological
406 phenotype to those of *Crtap*$^{-/-}$ mice[35]. These data are consistent with the principle that an altered
407 extracellular matrix can lead to altered cellular signaling as previously shown for vascular tissue
408 in Marfan syndrome and OI bone. Here, we extend this theme to tendon and ligamentous defects
409 in OI.

410 Collagen fibril assembly is a dynamic process that begins with the formation of many
411 small fibrils that grow longitudinally during development, followed by appositional fusion and
412 continued longitudinal growth as tendons mature[4]. In the present study, we found an increased
413 proportion of small and large collagen fibrils in the FDL and Achilles tendons as well as patellar
414 ligaments of *Crtap*$^{-/-}$ mice compared to wildtype. These distributions varied in severity across the

415 three tissues, with the greatest differences being observed in the patellar ligament. *Lepre1*$^{-/-}$ mice
416 have been reported to display an increased proportion of small collagen fibrils in tail tendons[19],
417 indicating that loss of the 3-prolyl hydroxylase complex alters collagen fibrillogenesis. At the
418 same time, the increased number of small fibers was more pronounced in *Lepre1*$^{-/-}$ mice, and
419 there was no evidence of an increased proportion of large fibers[19] as observed for *Crtap*$^{-/-}$ mice in
420 this study. Similar to the *Lepre1*$^{-/-}$ mouse model, mice lacking CypB also exhibit a pronounced
421 increase in the number of small collagen fibrils within tail tendons[18]. Together, this suggests that
422 despite forming a complex with P3h1 and CypB, loss of Crtap has distinct consequences on
423 collagen fibrillogenesis. In this regard, it is important to note that tail tendons were used for
424 collagen fibril distribution assessments in both *Lepre1*$^{-/-}$ and *Ppib*$^{-/-}$ mice[18, 19], whereas
425 appendicular tendons and ligaments were examined in our study. The difference in tissue type
426 examined might also explain why we observed unique alterations in collagen fibril distribution in
427 heterozygous *Crtap* mice, whereas *CypB* heterozygous tendons were indistinguishable from
428 wildtype[18].

429 Type I procollagen molecules undergo post-translational modifications within the
430 endoplasmic reticulum, including lysyl-hydroxylation and prolyl-hydroxylation, that are critical
431 for proper collagen synthesis, transport, and stability. Specifically, telopeptide lysine
432 hydroxylation results in mature lysyl-pyridinoline (LP) or hydroxylysyl-pyridinoline (HP)
433 residues after lysyl oxidase oxidation, which as permanent, irreversible crosslinks play a role in
434 regulating fibril growth and strength[25, 36]. Previous literature has demonstrated that loss of the 3-
435 prolyl hydroxylase complex caused by deletion of P3h1 (*Lepre1*$^{-/-}$) or Crtap (*Crtap*$^{-/-}$) prevents
436 prolyl 3-hydroxylation of clade A (type I, II and III) collagens and can lead to changes in lysine
437 post-translational modifications due to loss of its chaperone function[10, 11]. In this study, we found

438 that mature collagen cross-links (HP residues per collagen) are markedly increased in the FDL
439 and Achilles tendons as well as the patellar ligament of *Crtap*$^{-/-}$ mice relative to wildtype.
440 Interestingly, we observed increased cross-links in the Achilles, but not FDL or patellar tendons
441 of 1-month old heterozygous mice, indicating a mild haploinsufficient effect of Crtap on this
442 tendon biochemical property thereby suggesting a rate-limited contribution of this complex in
443 this function. Outside of the genotype-specific effects, we saw an age-dependent increase in HP
444 residues per collagen in all genotypes. This observation is consistent with a study by Taga and
445 colleagues that reported an increase in 3-hydroxyproline residues in rat tendon collagen (but not
446 bone or skin) that plateaued at 3 months-of-age[37]. Together with the TEM analyses, these data
447 suggest that altered collagen cross-linking in tendons and ligaments from *Crtap*$^{-/-}$ mice may
448 adversely affect collagen fibril assembly.

449 In addition to skeletal deformities and frequent fractures, severe OI is associated with
450 motor impairments including gait abnormalities, chronic pain, and reduced muscle strength[8, 9, 38].
451 In this study, we showed that *Crtap*$^{-/-}$ mice exhibit reduced motor activity and coordination using
452 the open field, rotarod, and grid foot slip assays. We also observed a reduction in latency to fall
453 on the inverted grid assay that was mirrored by a dramatic loss of grip strength compared to
454 heterozygous and wildtype mice. These results are consistent with findings reported for the
455 *Col1a1*$^{Jrt/+}$ mouse model of severe OI and Ehlers-Danlos syndrome[17]. Specifically, Abdelaziz
456 and colleagues found that *Col1a1*$^{Jrt/+}$ mice displayed reduced motor activity using the open field
457 and running wheel assays – a phenotype they attributed to thermal hyperalgesia and mechanical
458 allodynia in these mice[39]. In this regard, the reduced vertical activity we observed in *Crtap*$^{-/-}$
459 mice may be indicative of a pain or spinal phenotype, suggesting that the characterization of pain
460 in this model is a useful avenue for future research. Overall, this study represents one of the first

extensive characterizations of behavioral deficits in a mouse model of severe, recessive OI that also correlates these deficits to tendon phenotypes.

Taken together, this study provides the first evidence for tendon and ligament phenotypes in the *Crtap*$^{-/-}$ mouse model of severe recessive OI. We also provide compelling evidence for a strong motor activity and coordination phenotype in these mice. As the quality of life is so impacted in patients with OI, a more comprehensive evaluation of behavioral outcomes in future preclinical studies may provide important insights into the efficacy of therapeutic interventions.

AUTHOR CONTRIBUTIONS

M. W. Grol: Conception and design of the study, acquisition, analysis and interpretation of data, drafting and editing of the manuscript

N. A. Haelterman: Acquisition and analysis of data, editing of the manuscript

J. Lim: Acquisition and analysis of data, editing of the manuscript

E. Munivez: Acquisition of data

M. Archer: Acquisition and analysis of data

D. M. Hudson: Acquisition, analysis, and interpretation of data, editing of the manuscript

S. F. Tufa: Acquisition and analysis of data

D. R. Keene: Acquisition, analysis, and interpretation of data, editing of the manuscript

K. Lei: Acquisition and analysis of data

D. Park: Analysis and interpretation of data

D. R. Eyre: Analysis and interpretation of data, editing of the manuscript

B H. Lee: Conception and design of the study, interpretation of data, editing of the manuscript

484 **Competing Interests**

485 No competing interests to report.

486

487 **Funding**

488 BCM Intellectual and Developmental Disabilities Research Center (HD024064) from the Eunice
489 Kennedy Shriver National Institute Of Child Health & Human Development, the Rolanette and
490 Berdon Lawrence Bone Disease Program of Texas, the BCM Center for Skeletal Medicine and
491 Biology, and the Pamela and David Ott Center for Heritable Disorders of Connective Tissue. D.
492 Eyre was supported by a NIAMS R37 (AR37318).

493

494 **REFERENCES**

495 1. Nourissat G, Berenbaum F, Duprez D. Tendon injury: from biology to tendon repair. Nat Rev
496 Rheumatol 2015; 11: 223-233.
497 2. Screen HR, Berk DE, Kadler KE, Ramirez F, Young MF. Tendon functional extracellular
498 matrix. J Orthop Res 2015; 33: 793-799.
499 3. Kannus P. Structure of the tendon connective tissue. Scand J Med Sci Sports 2000; 10: 312-
500 320.
501 4. Kalson NS, Lu Y, Taylor SH, Starborg T, Holmes DF, Kadler KE. A structure-based
502 extracellular matrix expansion mechanism of fibrous tissue growth. Elife 2015; 4.
503 5. Saito M, Marumo K. Collagen cross-links as a determinant of bone quality: a possible
504 explanation for bone fragility in aging, osteoporosis, and diabetes mellitus. Osteoporos Int
505 2010; 21: 195-214.

506 6. Alford AI, Kozloff KM, Hankenson KD. Extracellular matrix networks in bone remodeling.
507 Int J Biochem Cell Biol 2015; 65: 20-31.
508 7. Lim J, Grafe I, Alexander S, Lee B. Genetic causes and mechanisms of osteogenesis
509 imperfecta. Bone 2017; 102: 40-49.
510 8. Arponen H, Makitie O, Waltimo-Siren J. Association between joint hypermobility, scoliosis,
511 and cranial base anomalies in paediatric osteogenesis imperfecta patients: a retrospective
512 cross-sectional study. BMC Musculoskelet Disord 2014; 15: 428.
513 9. Primorac D, Anticevic D, Barisic I, Hudetz D, Ivkovic A. Osteogenesis imperfecta--multi-
514 systemic and life-long disease that affects whole family. Coll Antropol 2014; 38: 767-772.
515 10. Hudson DM, Eyre DR. Collagen prolyl 3-hydroxylation: a major role for a minor post-
516 translational modification? Connect Tissue Res 2013; 54: 245-251.
517 11. Morello R, Bertin TK, Chen Y, Hicks J, Tonachini L, Monticone M, et al. CRTAP is
518 required for prolyl 3- hydroxylation and mutations cause recessive osteogenesis imperfecta.
519 Cell 2006; 127: 291-304.
520 12. Baldridge D, Schwarze U, Morello R, Lennington J, Bertin TK, Pace JM, et al. CRTAP and
521 LEPRE1 mutations in recessive osteogenesis imperfecta. Hum Mutat 2008; 29: 1435-1442.
522 13. Barnes AM, Chang W, Morello R, Cabral WA, Weis M, Eyre DR, et al. Deficiency of
523 cartilage-associated protein in recessive lethal osteogenesis imperfecta. N Engl J Med 2006;
524 355: 2757-2764.
525 14. Cabral WA, Chang W, Barnes AM, Weis M, Scott MA, Leikin S, et al. Prolyl 3-hydroxylase
526 1 deficiency causes a recessive metabolic bone disorder resembling lethal/severe
527 osteogenesis imperfecta. Nat Genet 2007; 39: 359-365.

528 15. van Dijk FS, Nesbitt IM, Zwikstra EH, Nikkels PG, Piersma SR, Fratantoni SA, et al. PPIB
529 mutations cause severe osteogenesis imperfecta. Am J Hum Genet 2009; 85: 521-527.
530 16. Baldridge D, Lennington J, Weis M, Homan EP, Jiang MM, Munivez E, et al. Generalized
531 connective tissue disease in *Crtap*$^{-/-}$ mouse. PLoS One 2010; 5: e10560.
532 17. Chen F, Guo R, Itoh S, Moreno L, Rosenthal E, Zappitelli T, et al. First mouse model for
533 combined osteogenesis imperfecta and Ehlers-Danlos syndrome. J Bone Miner Res 2014; 29:
534 1412-1423.
535 18. Terajima M, Taga Y, Chen Y, Cabral WA, Hou-Fu G, Srisawasdi S, et al. Cyclophilin-B
536 modulates collagen cross-linking by differentially affecting lysine hydroxylation in the
537 helical and telopeptidyl domains of tendon type I collagen. J Biol Chem 2016; 291: 9501-
538 9512.
539 19. Vranka JA, Pokidysheva E, Hayashi L, Zientek K, Mizuno K, Ishikawa Y, et al. Prolyl 3-
540 hydroxylase 1 null mice display abnormalities in fibrillar collagen-rich tissues such as
541 tendons, skin, and bones. J Biol Chem 2010; 285: 17253-17262.
542 20. Schindelin J, Arganda-Carreras I, Frise E, Kaynig V, Longair M, Pietzsch T, et al. Fiji: an
543 open-source platform for biological-image analysis. Nat Methods 2012; 9: 676-682.
544 21. Nixon AJ, Grol MW, Lang HM, Ruan MZC, Stone A, Begum L, et al. Disease-modifying
545 osteoarthritis treatment with interleukin-1 receptor antagonist gene therapy in small and large
546 animal models. Arthritis Rheumatol 2018; 70: 1757-1768.
547 22. Ruan MZ, Erez A, Guse K, Dawson B, Bertin T, Chen Y, et al. Proteoglycan 4 expression
548 protects against the development of osteoarthritis. Sci Transl Med 2013; 5: 176ra134.

549 23. Ruan MZ, Patel RM, Dawson BC, Jiang MM, Lee BH. Pain, motor and gait assessment of
550 murine osteoarthritis in a cruciate ligament transection model. Osteoarthritis Cartilage 2013;
551 21: 1355-1364.
552 24. Stone A, Grol MW, Ruan MZC, Dawson B, Chen Y, Jiang MM, et al. Combinatorial *Prg4*
553 and *Il-1ra* gene therapy protects against hyperalgesia and cartilage degeneration in post-
554 traumatic osteoarthritis. Hum Gene Ther 2019; 30: 225-235.
555 25. Eyre D. Collagen cross-linking amino acids. Methods Enzymol 1987; 144: 115-139.
556 26. Hudson DM, Archer M, King KB, Eyre DR. Glycation of type I collagen selectively targets
557 the same helical domain lysine sites as lysyl oxidase-mediated cross-linking. J Biol Chem
558 2018; 293: 15620-15627.
559 27. Steinmann S, Pfeifer CG, Brochhausen C, Docheva D. Spectrum of tendon pathologies:
560 triggers, trails and end-state. Int J Mol Sci 2020; 21.
561 28. Dyment NA, Hagiwara Y, Matthews BG, Li Y, Kalajzic I, Rowe DW. Lineage tracing of
562 resident tendon progenitor cells during growth and natural healing. PLoS One 2014; 9:
563 e96113.
564 29. Dyment NA, Liu CF, Kazemi N, Aschbacher-Smith LE, Kenter K, Breidenbach AP, et al.
565 The paratenon contributes to scleraxis-expressing cells during patellar tendon healing. PLoS
566 One 2013; 8: e59944.
567 30. Howell K, Chien C, Bell R, Laudier D, Tufa SF, Keene DR, et al. Novel model of tendon
568 regeneration reveals distinct cell mechanisms underlying regenerative and fibrotic tendon
569 healing. Sci Rep 2017; 7: 45238.

570 31. Harvey T, Flamenco S, Fan CM. A Tppp3(+)Pdgfra(+) tendon stem cell population
571 contributes to regeneration and reveals a shared role for PDGF signalling in regeneration and
572 fibrosis. Nat Cell Biol 2019; 21: 1490-1503.
573 32. Lee CH, Lee FY, Tarafder S, Kao K, Jun Y, Yang G, et al. Harnessing endogenous
574 stem/progenitor cells for tendon regeneration. J Clin Invest 2015; 125: 2690-2701.
575 33. Feng H, Xing W, Han Y, Sun J, Kong M, Gao B, et al. Tendon-derived cathepsin K-
576 expressing progenitor cells activate Hedgehog signaling to drive heterotopic ossification. J
577 Clin Invest 2020.
578 34. Grafe I, Yang T, Alexander S, Homan EP, Lietman C, Jiang MM, et al. Excessive
579 transforming growth factor-beta signaling is a common mechanism in osteogenesis
580 imperfecta. Nat Med 2014; 20: 670-675.
581 35. Lim J, Munivez E, Jiang MM, Song IW, Gannon F, Keene DR, et al. mTORC1 Signaling is a
582 critical regulator of postnatal tendon development. Sci Rep 2017; 7: 17175.
583 36. Bateman JF, Boot-Handford RP, Lamande SR. Genetic diseases of connective tissues:
584 cellular and extracellular effects of ECM mutations. Nat Rev Genet 2009; 10: 173-183.
585 37. Taga Y, Kusubata M, Ogawa-Goto K, Hattori S. Developmental stage-dependent regulation
586 of prolyl 3-hydroxylation in tendon type I collagen. J Biol Chem 2016; 291: 837-847.
587 38. Garman CR, Graf A, Krzak J, Caudill A, Smith P, Harris G. Gait deviations in children with
588 osteogenesis imperfecta type I. J Pediatr Orthop 2019; 39: e641-e646.
589 39. Abdelaziz DM, Abdullah S, Magnussen C, Ribeiro-da-Silva A, Komarova SV, Rauch F, et
590 al. Behavioral signs of pain and functional impairment in a mouse model of osteogenesis
591 imperfecta. Bone 2015; 81: 400-406.

592

593 **FIGURE LEGENDS**

594 Figure 1. **Loss of Crtap causes thinning and hypercellularity of tendons and ligaments in**
595 **young and mature mice. (A-C)** representative H&E images of 1-month ankle joints. **(D-F)**,
596 representative H&E images of 1-month knee joints. **(G-I)** representative H&E images of 4-
597 month ankle joints. **(J-L)** representative H&E images of 4-month knee joints. For all
598 micrographs, higher magnification images of the mid-tendon/ligament are illustrated. n = 3-4
599 mice per group. Scale bar is 1-mm. **(M-N)** quantification of cell density for Achilles tendons and
600 patellar ligaments of wildtype and *Crtap*$^{-/-}$ mice at 1-month **(M)** and 4-months **(N)** of age. Data
601 are min-to-max box and whisker plots with individual points indicated. n = 3 mice per group.
602 Data passed the Shapiro-Wilk test for normality, and groups were compared using two-tailed
603 unpaired t-tests. Exact *p*-values are reported. **(O-P)** representative phase-contrast μCT images of
604 4-month wildtype **(O)** and *Crtap*$^{-/-}$ **(P)** knee joints. Blue indicates the patellar ligament, green
605 indicates the femoral articular cartilage, and red indicates the tibial articular cartilage. Scale bar
606 is 1-mm. **(Q)** volumetric quantification of the patellar ligament volume in wildtype,
607 heterozygous, and *Crtap*$^{-/-}$ mice. Data are min-to-max box and whisker plots with individual
608 points indicated. n = 3 mice per group. Data passed the Shapiro-Wilk test for normality, and
609 groups were compared using one-way ANOVA with Tukey's post-hoc tests. Exact *p*-values are
610 reported.

611

612 Figure 2. **Loss of Crtap in patellar ligaments leads to a decrease in progenitor cells and an**
613 **accumulation of immature resident tissue cells. (A-B)** patellar ligament cells isolated from 5-
614 month-old wildtype **(A)** or *Crtap*$^{-/-}$ **(B)** mice were analyzed for the expression of CD200 and
615 CD146 tendon/ligament progenitor markers (*top histogram*) within the CD45^{-}CD31^{-} population

616 (*bottom histogram*). The plots are representative from a single wildtype or *Crtap*$^{-/-}$ mouse. **(C-D)**
617 graphs show the percentage of CD45^{-}CD31^{-}CD146^{+}CD200^{+} progenitor cells **(C)** and CD45^{-}
618 CD31^{-}CD146^{-}CD200^{+} immature ligament cells **(D)** from 5-month wildtype and *Crtap*$^{-/-}$ patellar
619 ligaments. Data are min-to-max box and whisker plots with individual points indicated. n = 5
620 mice per group. Data passed the Shapiro-Wilk test for normality, and groups were compared
621 using two-tailed unpaired t-tests. Exact *p*-values are reported.
622
623 Figure 3. **Collagen fibril diameter is altered in tendons and ligaments from heterozygous**
624 **and *Crtap*$^{-/-}$ mice. (A-C)** representative TEM images of 4-month FDL tendon collagen fibrils.
625 Scale bar is 500-nm. **(D)** representative histogram of the size distribution for collagen fibrils in
626 FDL tendons. Data are representative of n = 3 mice. **(E-G)** representative TEM images of 4-
627 month Achilles tendon collagen fibrils. Scale bar is 500-nm. **(H)** representative histogram of the
628 size distribution for collagen fibrils in Achilles tendons. Data are representative of n = 3 mice. **(I-**
629 **K)** representative TEM images of 4-month patellar ligament collagen fibrils. Scale bar is 500-
630 nm. **(L)** representative histogram of the size distribution for collagen fibrils in patellar ligaments.
631 Data are representative of n = 3 mice per group.
632
633 Figure 4. **Collagen cross-linking is increased in tendons and ligaments from young and**
634 **mature *Crtap*$^{-/-}$ mice.** Quantification of collagen cross-links as hydroxylysyl-pyridinoline (HP)
635 residues per collagen molecule for **(A)** FDL tendons; **(B)** Achilles tendons; and **(C)** patellar
636 ligaments. Data are shown as means ± S.D. n = 3-4 mice per group. Data passed the Shapiro-
637 Wilk test for normality, and groups were compared using one-way ANOVA with Tukey's post-
638 hoc tests. Exact *p*-values are reported.

639 Figure 5. **Transcriptome analysis of tendons and ligaments from 1-month-old *Crtap*$^{-/-}$ mice.**
640 DESeq2 was used to compare gene expression between wildtype and *Crtap*$^{-/-}$ Achilles tendon
641 and patellar ligament RNA samples, and genes with an adjusted *p*-value < 0.05 and absolute $\log_2$
642 fold change > 1 were considered as differentially expressed. **(A)** a bi-clustering heatmap of the
643 top 30 differentially expressed genes between wildtype and *Crtap*$^{-/-}$ Achilles tendons sorted by
644 adjusted *p*-value and plotted according to $\log_2$ transformed expression values. The Wald test was
645 used to generate p-values and $\log_2$ fold changes. **(B)** significantly differentially expressed genes
646 between Achilles tendons from wildtype and *Crtap*$^{-/-}$ mice were clustered by their gene ontology,
647 and enrichment for gene ontology terms was tested using Fisher exact test. All gene ontology
648 terms with an adjusted *p*-value < 0.05 are plotted according to their $-\log_{10}$ adjusted *p*-value. **(C)**
649 select upstream regulators predicted as being activated (shown in green), inhibited (shown in
650 red), or of unclear state (shown in grey) in *Crtap*$^{-/-}$ compared to wildtype Achilles tendons plotted
651 according to their $-\log_{10}$ adjusted *p*-value. n = 3 mice per genotype for **(A-C)**. **(D)** a bi-clustering
652 heatmap of the top 30 differentially expressed genes between wildtype and *Crtap*$^{-/-}$ patellar
653 ligaments sorted by adjusted *p*-value and plotted according to $\log_2$ transformed expression
654 values. The Wald test was used to generate p-values and $\log_2$ fold changes. **(E)** significantly
655 differentially expressed genes between Achilles tendons from wildtype and *Crtap*$^{-/-}$ mice were
656 clustered by their gene ontology, and enrichment for gene ontology terms was tested using Fisher
657 exact test. All gene ontology terms with an adjusted *p*-value < 0.05 are plotted according to their
658 $-\log_{10}$ adjusted *p*-value. **(F)** select upstream regulators predicted as being activated (shown in
659 green), inhibited (shown in red), or of unclear state (shown in grey) in *Crtap*$^{-/-}$ compared to
660 wildtype patellar ligaments plotted according to $-\log_{10}$ adjusted *p*-value. n = 2 mice per genotype
661 for **(D-F)**.

662 Figure 6. **Motor activity and coordination are impaired in 4-months-old *Crtap*$^{-/-}$ mice. (A-B)**
663 quantification of spontaneous motor activity including horizontal **(A)** and vertical **(B)** activity
664 over a 30-min period using the open field assay. Data are min-to-max box and whisker plots with
665 individual points indicated. n = 9-12 mice per group. For **(A)**, data passed the Shapiro-Wilk test
666 for normality, and groups were compared using one-way ANOVA with Tukey's post-hoc tests.
667 For **(B)**, data failed the Shapiro-Wilk test for normality, and groups were compared using
668 Kruskal-Wallis with Dunn's post-hoc tests. Exact p-values are reported for **(A-B)**. **(C)**
669 quantification of motor activity, coordination, and endurance across 10 trials conducted over 2
670 days using an accelerating rotarod assay. Data are means ± S.D. n = 9-12 mice per group. Groups
671 were compared using repeated-measures two-way ANOVA with Tukey's post-hoc tests. Exact *p*-
672 values are reported, with black *p*-values being compared to wildtype, and blue *p*-values being
673 compared to heterozygous mice. **(D-E)** quantification of forelimb **(D)** and hindlimb **(E)** motor
674 coordination using the grid foot slip assay. Data are min-to-max box and whisker plots with
675 individual points indicated. n = 9-11 mice per group. Data failed the Shapiro-Wilk test for
676 normality, and groups were compared using Kruskal-Wallis with Dunn's post-hoc tests. Exact p-
677 values are reported. **(F)** quantification of forelimb and hindlimb grip strength using the inverted
678 grid assay conducted for 120 s. A reduction in latency to fall indicates reduced strength. Data are
679 min-to-max box and whisker plots with individual points indicated. n = 8-9 mice per group. Data
680 failed the Shapiro-Wilk test for normality, and groups were compared using Kruskal-Wallis with
681 Dunn's post-hoc tests. Exact p-values are reported. **(G)** quantification of forelimb grip strength
682 in N of force measured over 3 trials and then averaged. Data are min-to-max box and whisker
683 plots with individual points indicated. n = 9-12 mice per group. Data passed the Shapiro-Wilk
684 test for normality, and groups were compared using one-way ANOVA with Tukey's post-hoc

685 tests. Exact *p*-values are reported.

FIGURE 1

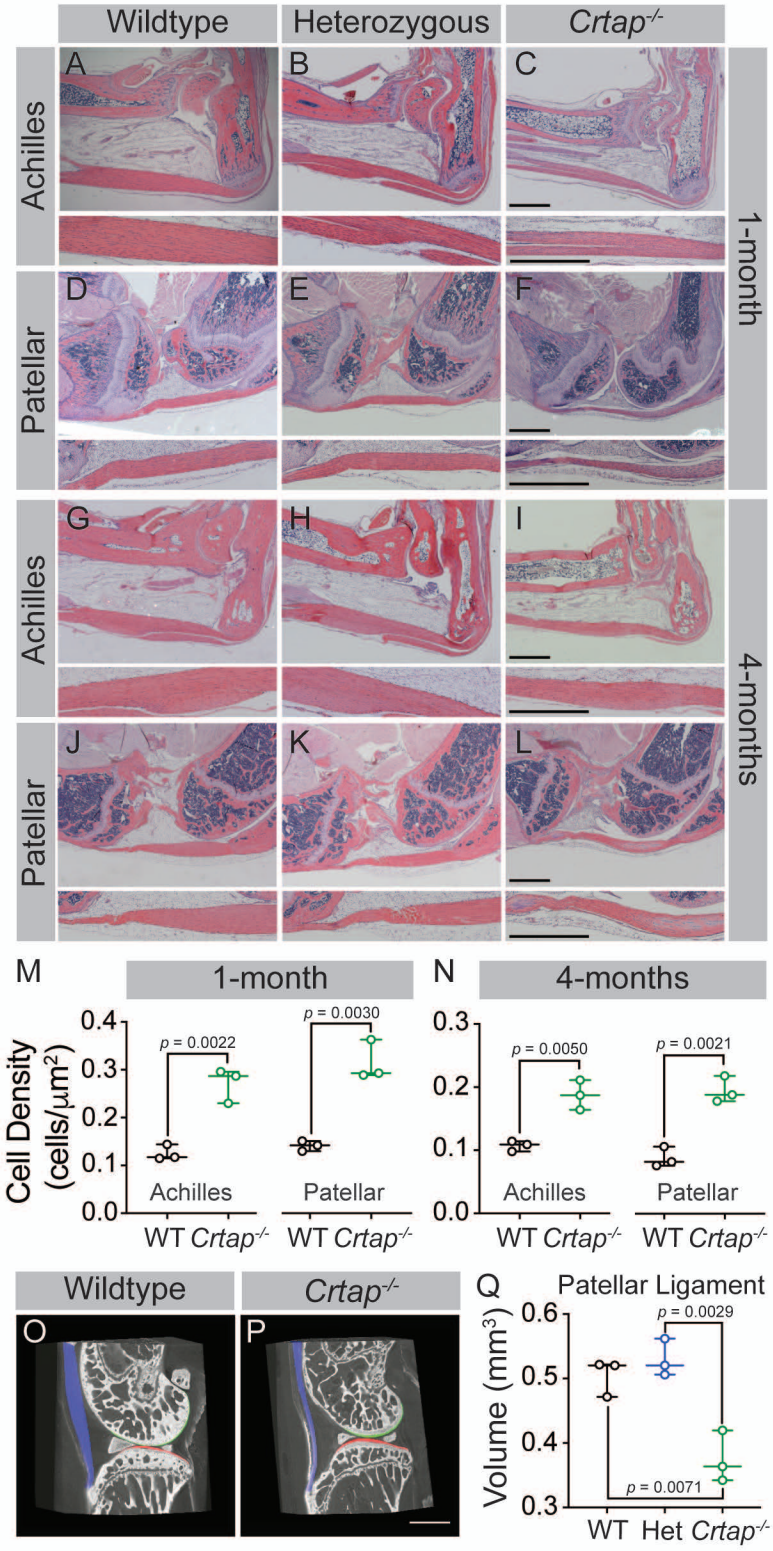
Wildtype
Heterozygous
Crtap-/-
Achilles
Patellar
1-month
4-months
A
B
C
D
E
F
G
H
I
J
K
L
M
1-month
N
4-months
Cell Density (cells/μm²)
p = 0.0022
p = 0.0030
p = 0.0050
p = 0.0021
Achilles
Patellar
WT Crtap-/-
O
P
Q
Patellar Ligament
Volume (mm³)
p = 0.0029
p = 0.0071
WT Het Crtap-/-

FIGURE 2

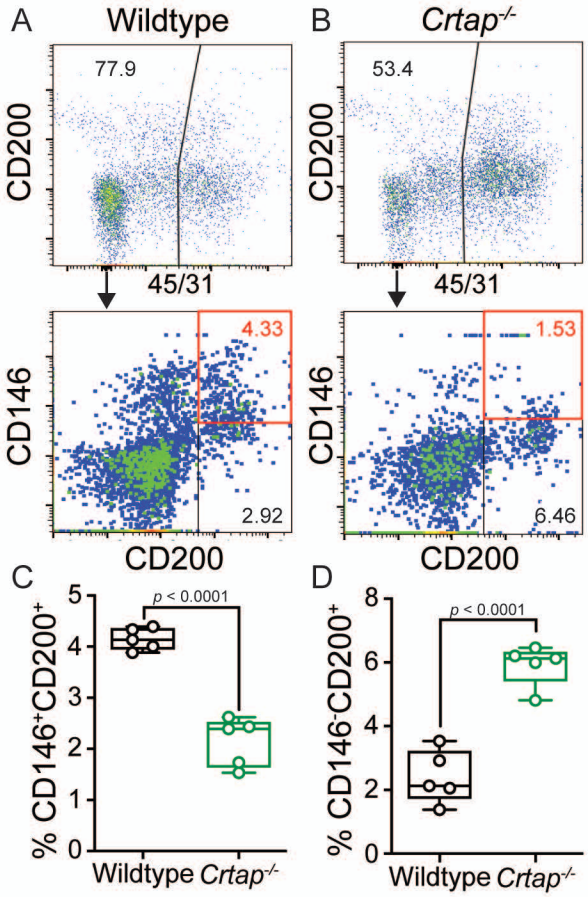
A
Wildtype
B
Crtap-/-
77.9
53.4
CD200
45/31
4.33
1.53
CD146
2.92
6.46
CD200
C
D
p < 0.0001
% CD146+CD200+
% CD146-CD200+
Wildtype
Crtap-/-

FIGURE 3

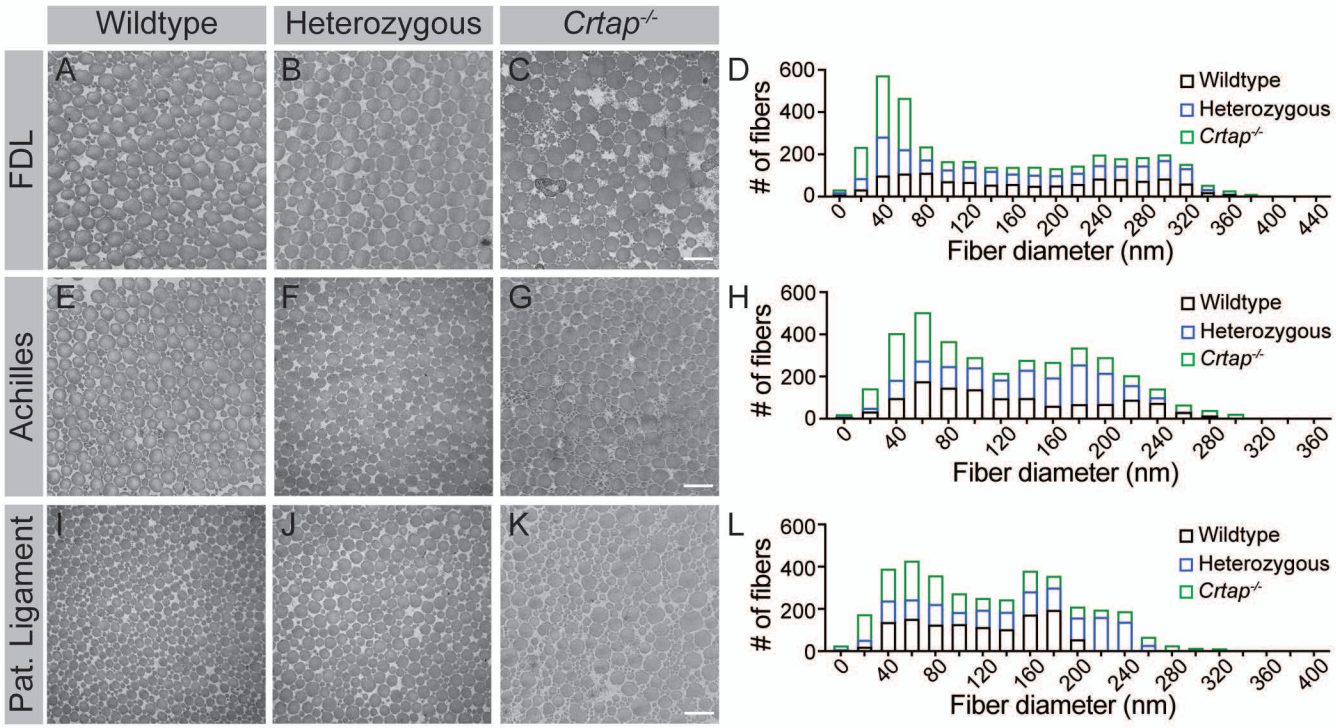
Wildtype
Heterozygous
Crtap-/-
FDL
Achilles
Pat. Ligament
A
B
C
D
E
F
G
H
I
J
K
L
# of fibers
Fiber diameter (nm)
Wildtype
Heterozygous
Crtap-/-

FIGURE 4

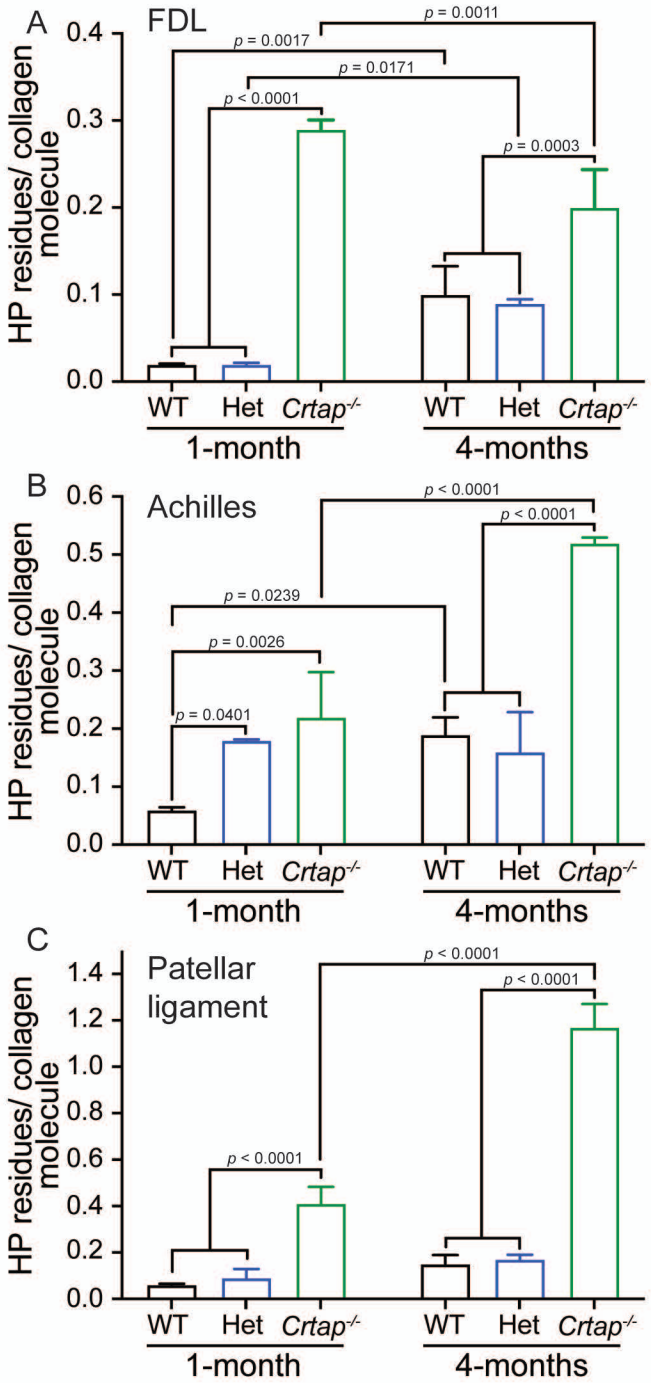
A
FDL
HP residues/ collagen molecule
0.4
0.3
0.2
0.1
0.0
p = 0.0011
p = 0.0017
p = 0.0171
p < 0.0001
p = 0.0003
WT
Het
Crtap-/-
WT
Het
Crtap-/-
1-month
4-months
B
Achilles
HP residues/ collagen molecule
0.6
0.5
0.4
0.3
0.2
0.1
0.0
p < 0.0001
p < 0.0001
p = 0.0239
p = 0.0026
p = 0.0401
WT
Het
Crtap-/-
WT
Het
Crtap-/-
1-month
4-months
C
Patellar ligament
HP residues/ collagen molecule
1.4
1.2
1.0
0.8
0.6
0.4
0.2
0.0
p < 0.0001
p < 0.0001
p < 0.0001
WT
Het
Crtap-/-
WT
Het
Crtap-/-
1-month
4-months

FIGURE 5

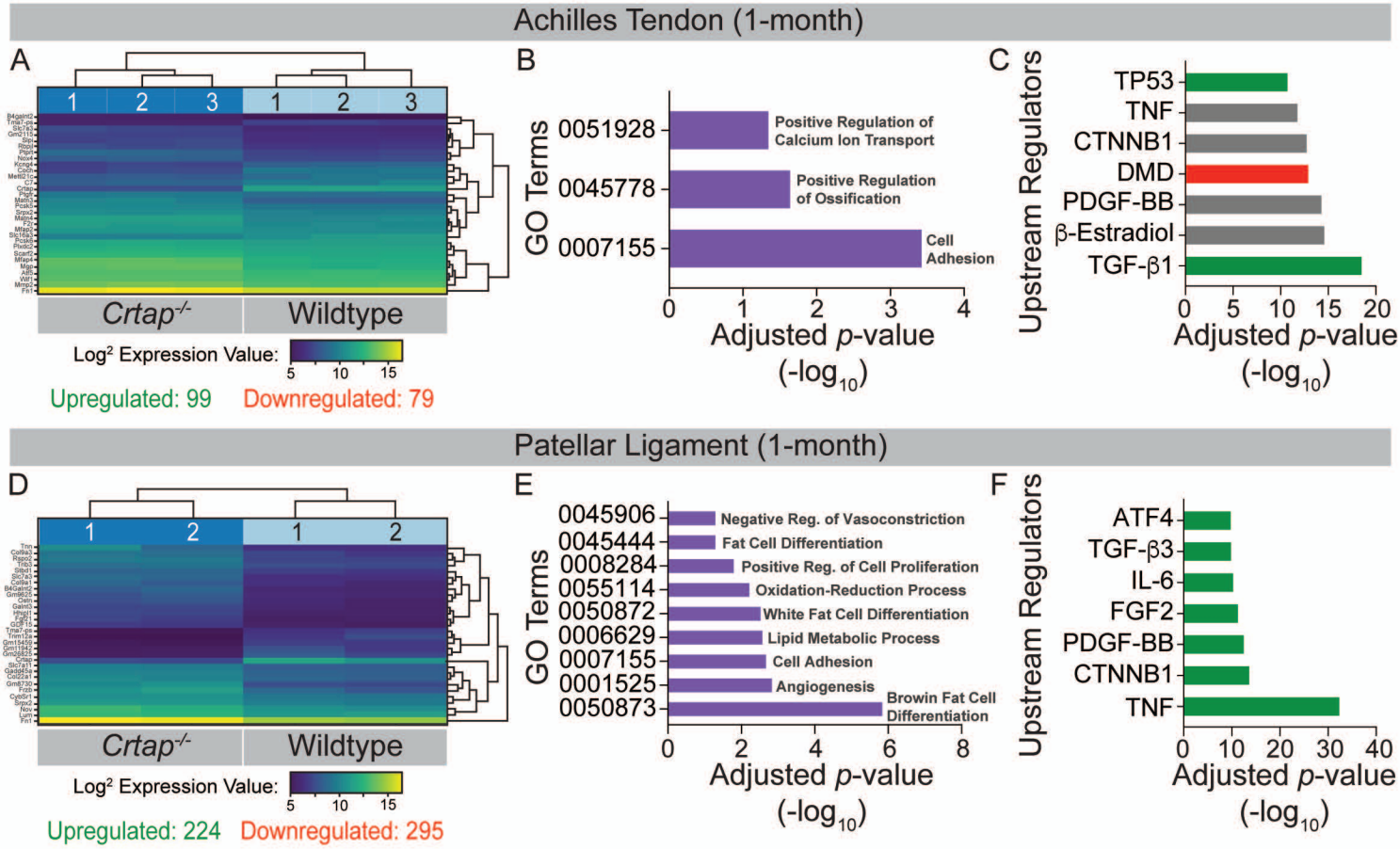
Achilles Tendon (1-month)
A
1 2 3 1 2 3
Crtap-/-
Wildtype
Log2 Expression Value:
5 10 15
Upregulated: 99
Downregulated: 79
B
GO Terms
0051928
0045778
0007155
Positive Regulation of Calcium Ion Transport
Positive Regulation of Ossification
Cell Adhesion
0 1 2 3 4
Adjusted p-value (-log10)
C
Upstream Regulators
TP53
TNF
CTNNB1
DMD
PDGF-BB
β-Estradiol
TGF-β1
0 5 10 15 20
Adjusted p-value (-log10)
Patellar Ligament (1-month)
D
1 2 1 2
Crtap-/-
Wildtype
Log2 Expression Value:
5 10 15
Upregulated: 224
Downregulated: 295
E
GO Terms
0045906
0045444
0008284
0055114
0050872
0006629
0007155
0001525
0050873
Negative Reg. of Vasoconstriction
Fat Cell Differentiation
Positive Reg. of Cell Proliferation
Oxidation-Reduction Process
White Fat Cell Differentiation
Lipid Metabolic Process
Cell Adhesion
Angiogenesis
Browin Fat Cell Differentiation
0 2 4 6 8
Adjusted p-value (-log10)
F
Upstream Regulators
ATF4
TGF-β3
IL-6
FGF2
PDGF-BB
CTNNB1
TNF
0 10 20 30 40
Adjusted p-value (-log10)

FIGURE 6

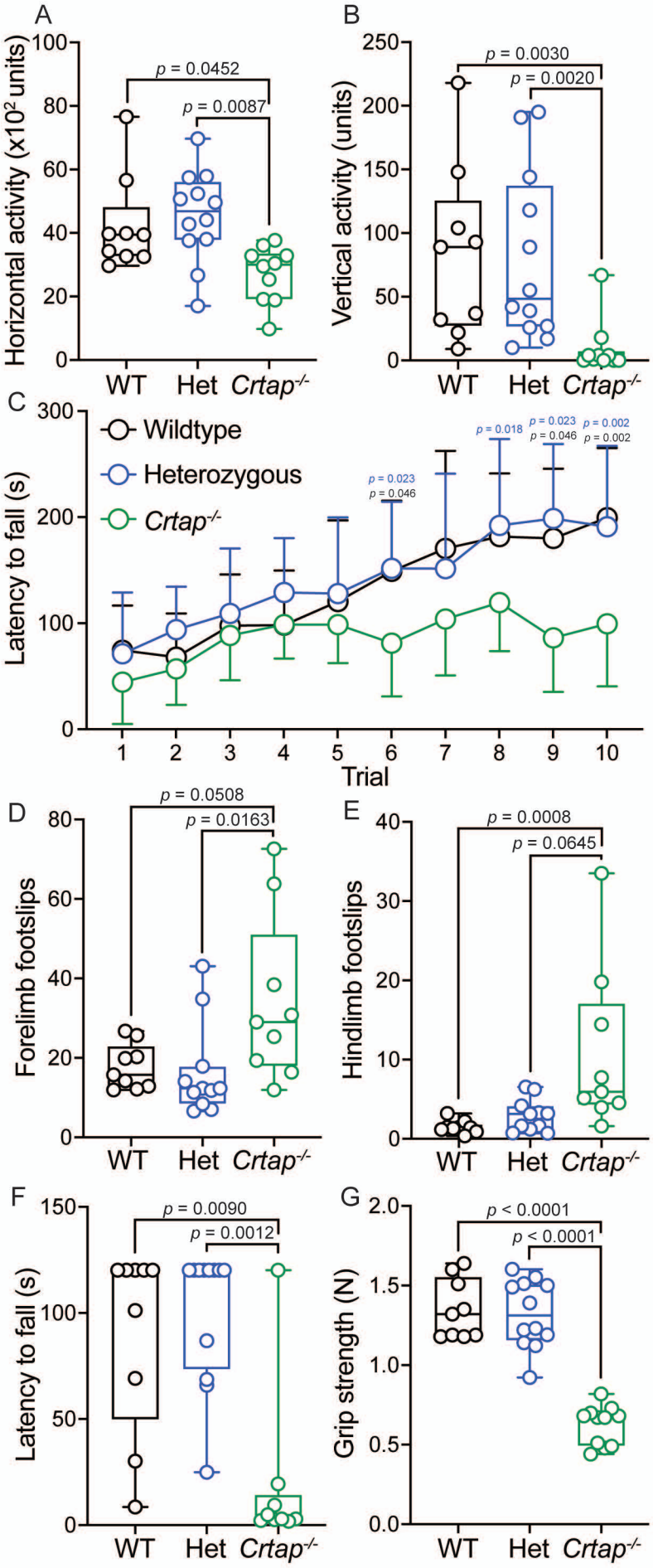
A
Horizontal activity (x10² units)
p = 0.0452
p = 0.0087
WT
Het
Crtap-/-
B
Vertical activity (units)
p = 0.0030
p = 0.0020
C
Latency to fall (s)
Wildtype
Heterozygous
Crtap-/-
p = 0.023
p = 0.046
p = 0.018
p = 0.023
p = 0.046
p = 0.002
p = 0.002
Trial
D
Forelimb footslips
p = 0.0508
p = 0.0163
E
Hindlimb footslips
p = 0.0008
p = 0.0645
F
Latency to fall (s)
p = 0.0090
p = 0.0012
G
Grip strength (N)
p < 0.0001
p < 0.0001